Carbohydrate Research 344 (2009) 1213–1224

Contents lists available at ScienceDirect

Carbohydrate Research

journal homepage: www.elsevier.com/locate/carres

Bidentate palladium(II) chelation by the common aldoses

Yvonne Arendt, Oliver Labisch, Peter Klüfers *

Department of Chemistry and Biochemistry, Ludwig-Maximilians-Universität, Butenandtstraße 5-13, D-81377 Munich, Germany

ARTICLE INFO

Article history:
Received 16 February 2009
Accepted 9 April 2009
Available online 12 April 2009

Keywords:
Aldoses
Monosaccharide chelates
Palladium
Dynamic equilibria

ABSTRACT

The [Pd^{II}{(*R*,*R*)-chxn}$(OH)_2$] reagent (chxn = 1,2-diaminocyclohexane) is introduced as a metal probe for the detection of the bidentate chelating sites of a glycose. Two moles of hydroxide per mole palladium support double deprotonation of potentially chelating diol functions at a glycose's backbone. The individual chelating sites are detected using one- and two-dimensional NMR techniques. At equimolar amounts of palladium(II) and aldose, the metal-binding sites include mostly the hydroxy function at the anomeric carbon atom. Chelators are derived from both the pyranose and the furanose isomers. Most pyranose-based chelators form five-membered chelate rings by using their 1,2-diol function. Though 1,2-diolate bonding is also common to the furanoses, the formation of six-membered chelate rings by 1,3-bonding is more significant for them. Metal-excess conditions provoke mostly bis-bidentate 1,2;3,4-chelation but unusual isomers form also: thus D-xylose is dimetallated in its all-axial β-pyranose form, and erythrose's dimetallation results in the formation of two isomers of a metal derivative of the open-chain hydrate. The spectroscopic results are supported by crystal-structure determinations on [Pd{(*R*,*R*)-chxn}(α-D-Xyl*p*1,2H_{-2}-κ$O^{1,2}$)]·H_2O (Xyl = xylose), [Pd{(*R*,*R*)-chxn}(α-D-Rib*p*1,2H_{-2}-κ$O^{1,2}$)]·2.25H_2O (Rib = ribose), [Pd{(*R*,*R*)-chxn}(α-L-Thr*f*1,3H_{-2}-κ$O^{1,3}$)]·2H_2O (Thr = threose) and [Pd{(*R*,*R*)-chxn}(α-D-Ery*f*1,3H_{-2}-κ$O^{1,3}$)]·3H_2O (Ery = erythrose).

1. Introduction

The evaluation of the ligand properties of carbohydrates has increased steadily over the past two decades. The majority of work has not been focused, however, on the parent carbohydrates, the glycoses, but has been focused on less reactive derivatives, mostly glycosides, including the nucleosides, glycositols or glyconic acids.[1] The reason, obviously, is the occurrence of both practical problems and conceptual peculiarities that are common to the members of the class of 'reducing sugars' which include the parent glycoses themselves, but also derivatives such as 2-deoxy-glycoses, glycuronic acids, the non-anomerically phosphorylated glycose phosphates, and glycosamines (2-deoxy-2-amino-glycoses).

The practical problems include the reactive carbohydrates' sensitivity in the alkaline regime as well as their reducing property. Thus, in the present work that is focused on palladium(II) chemistry, particularly the latter point results in the pronounced thermal instability of the investigated palladium(II)–glycose solutions. It should be noted that solutions that contain palladium(II)–glycose couples resemble the classical reagents for the detection of reducing sugars in terms of redox potentials and thus are prone to palladium(0) precipitation.

It is more challenging and more interesting, however, to master the conceptual consequence of attempting to use a reactive carbohydrate as a chelating ligand. In contrast to the standard ligands used in coordination chemistry, the solution of a single glycose does not provide only a single metal-binding site but provides numerous sites located at various isomers in a dynamic equilibrium. Using D-ribose as an example, Scheme 1 depicts a collection of species that may be considered bidentate chelators of some significance. Though limitations are introduced (bidentate chelation only, pyranose chairs only, no open-chain isomers, the most acidic OH1 group mandatorily contributing to each chelate ring), the considerable number of six potential chelators, including both furanose and pyranose forms with two of the latter being conformers, results.

The experimental conditions in recent attempts to probe a glycose's 'ligand library' are designed mostly to decrease the number of expected species efficiently. Examples include work by our group on ethylenediamine–palladium(II) complexes of monosaccharides, where full-metallation conditions were applied with the aim of excluding those isomers that are unable to provide a second metal-binding site.[2,3] However, the important issues of carbohydrate–metal chemistry are far from the special case of full metallation which is relevant in fields such as the construction of chiral coordination networks.[4] Thus, a contribution to issues such as homogenous metal catalysis as a tool for carbohydrate transformations can hardly be made as long as metal excess is applied. Instead, mononucleating metal binding is the typical binding situation in an attempted catalytic cycle. Similar arguments hold for the medicinal use of carbohydrate-based bioligand–metal chelates.

* Corresponding author. Fax: +89 2180 77407.
E-mail address: kluef@cup.uni-muenchen.de (P. Klüfers).

0008-6215/$ - see front matter © 2009 Elsevier Ltd. All rights reserved.
doi:10.1016/j.carres.2009.04.008

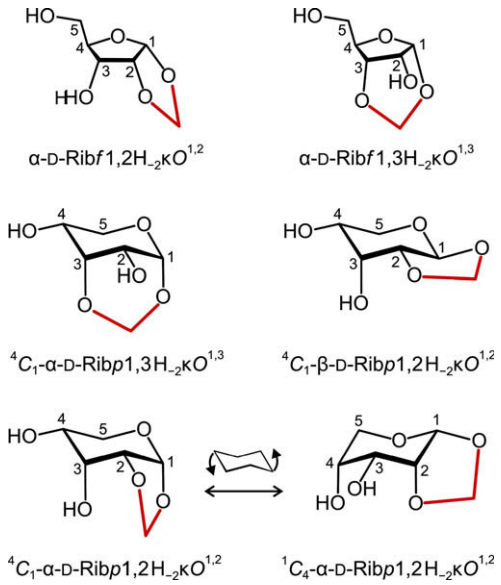

Scheme 1. Tentative bidentate chelators provided by a ribose dianion. The formulas in the bottom line represent conformers.

Yet unsolved experimental problems, however, have so far prohibited a comprehensive analysis of equimolar metal-to-glycose binding. D-Ribose, which was chosen as an introductory example, clearly shows both the problems and the challenges: probing the bidentate metal-binding sites provided by a ribose solution to a spectator-ligand–palladium(II) fragment (details are given in the first part of the Section 2.1) indicates four well-developed monometallated species in terms of NMR spectroscopy. Thus, a considerable subset of the six hypothetical bidentate chelators is obviously present as major equilibrium constituents. In fact, increasing the molar metal:ribose ratio produces only a single dimetallated ribose complex. This situation is typical: full-metallation conditions allow a first, but restricted, approach to the field, whereas the exploration of the many facets of glycose-metal chemistry needs tools powerful enough to include the equimolar metal:glycose regime.

We are here reporting on progress that has been made as a result of spectator-ligand diversification. In particular, the replacement of the initially applied 'Pd-en' agent, an aqueous solution of $[Pd(en)(OH)_2]$ (en = ethylenediamine), by the related chiral solvent termed 'Pd-chxn' led to a consistent body of data on the metal-binding sites of a glycose. Pd-chxn is an aqueous solution of (*R*,*R*)-cyclohexane-1,2-diamine-dihydroxido-palladium(II) and provides both the Pd^{II}{(*R*,*R*)-chxn} fragment as a probe for bidentate chelation sites of a tentative ligand and 2 equiv of base per palladium atom to achieve double deprotonation of the respective diol moiety. The term Pd-chxn follows the nomenclature of cellulose solvents, to which the new reagent belongs.[5]

The benefits of using the Pd-chxn reagent are demonstrated by a detailed analysis of equimolar palladium–aldose equilibria for the common aldoses. To explain the experimental strategy, the example ribose has been worked out in detail as an introductory case.

2. Results and discussion

2.1. Bidentate D-ribose chelators: an introduction to the strategy

In terms of standard ^{13}C NMR spectroscopy, aqueous ribose solutions consist of four isomers: α- and β-D-ribopyranose (α-D-Rib*p*, β-D-Rib*p*) as well as α- and β-D-ribofuranose (α-D-Rib*f*, β-D-Rib*f*). Since a maximum of two chelate rings can be provided by an aldopentose molecule, two metal:glycose molar ratios suffice to identify mono- and dimetallated species. The result of ribose reacting with an equimolar and a threefold molar amount of metal probe is shown in Figure 1 in terms of the C1 signal in ^{13}C NMR spectra of D-ribose equilibrium mixtures in Pd-chxn. Assigning signals to dimetallated species which increase from the ratio of 1:1 to 3:1 and signals to monometallated ones which decrease in the same order give the above-mentioned result. As a rule, full metallation significantly lowers the number of possible species. However, the unusual fact that ribose is atypical among the common aldoses in terms of the relative instability of its dimetallated species should be noted at this point. (Typically, a glycose gives rise to only small signals of monometallated species at as high a metal supply as 3:1 instead of to such well-developed signals of Pd_1Rib_1 species of the 'wrong' stoichiometry.)

Two-dimensional NMR techniques were used to elucidate the $^3J_{H,H}$ coupling constants as the basis for determining the configuration and conformation of the respective ligands (see Supplementary tables). As a result, two $\kappa O^{1,2}$ chelators and one $\kappa O^{1,3}$ chelator were assigned for the monometallated species, one of them derived from α-D-ribopyranose and two are derived from α-D-ribofuranose.

Taking 'coordination-induced shift' (CIS) values into account, the main species of the equimolar solutions is the Pd complex derived from the $^1C_4$-α-D-Rib*p*1,2H$_{-2}$-$\kappa O^{1,2}$ ligand. The major species is accompanied by two α-furanose ligands, the one binding in the $\kappa O^{1,2}$ mode, the other binding in the $\kappa O^{1,3}$ mode.

The main solution species at the 3:1 molar ratio was assigned, in agreement with the previous study on Pd-en, to the dimetallated $^4C_1$-β-D-Rib*p*H$_{-4}$-$\kappa O^{1,2}$:$\kappa O^{3,4}$ ligand.[2] If the general result of the spectrometric analysis of the other aldoses is taken into account—that very similar chemical shifts of related mono- and dimetallated forms should be observed for the C1 atom, which is distant from the binding site of the second metal atom—the small signal close to 101 ppm may be assigned to the 1,2-monometallated analogue of the dimetallated species. We assume that other small signals in the equimolar case come from complexes with a non-metal-bonding oxygen atom at the 1-position.

Among the stronger signals, one case remained unclear: due to signal overlap in correlated spectra, we were unable to assign the rightmost C1 signal shown in Figure 1. In terms of similarity to the all-axial xylose isomer discussed below, $^4C_1$-β-D-Rib*p* appears to be a sensible assignment. Two metal-binding sites appear reasonable: $\kappa O^{1,3}$-binding more closely resembles the dimetallated xylopyranose isomer, whereas $\kappa O^{3,4}$-binding, including an intramolecular O1–H···O3 hydrogen bond, would resemble binding in the 1:1 solution's major isomer. (In fact, the analysis of arabinose adds evidence for the $\kappa O^{1,3}$-chelator; see below.)

A comment on the chemical shifts caused by diolate–palladium(II) binding, the 'coordination-induced shifts' (CISs), should be given at this point. Throughout this work, the general rules as known from previous work on sugar alcohols and glycosides as well as on fully metallated glycoses, are valid: in the case of a five-membered chelate ring, the signals of the carbon atoms experience an approximately 10-ppm downfield shift relative to the free chelator. In the case of a six-membered chelate ring, markedly smaller CISs are observed (Tables 2 and 3).[2]

Though correlated NMR techniques allow signal assignment at a high level of confidence, independent proof of the conclusions drawn is, of course, desirable. Since the solubility of the various complexes appears to be almost the same for all species, as a very rough rule of thumb, the most abundant species of an equilibrium mixture is the most likely to crystallise on oversaturation. Accordingly, the major species of equimolar solutions of Pd-chxn and D-ribose crystallised as the 2.25-hydrate: [Pd{(*R*,*R*)-chxn}

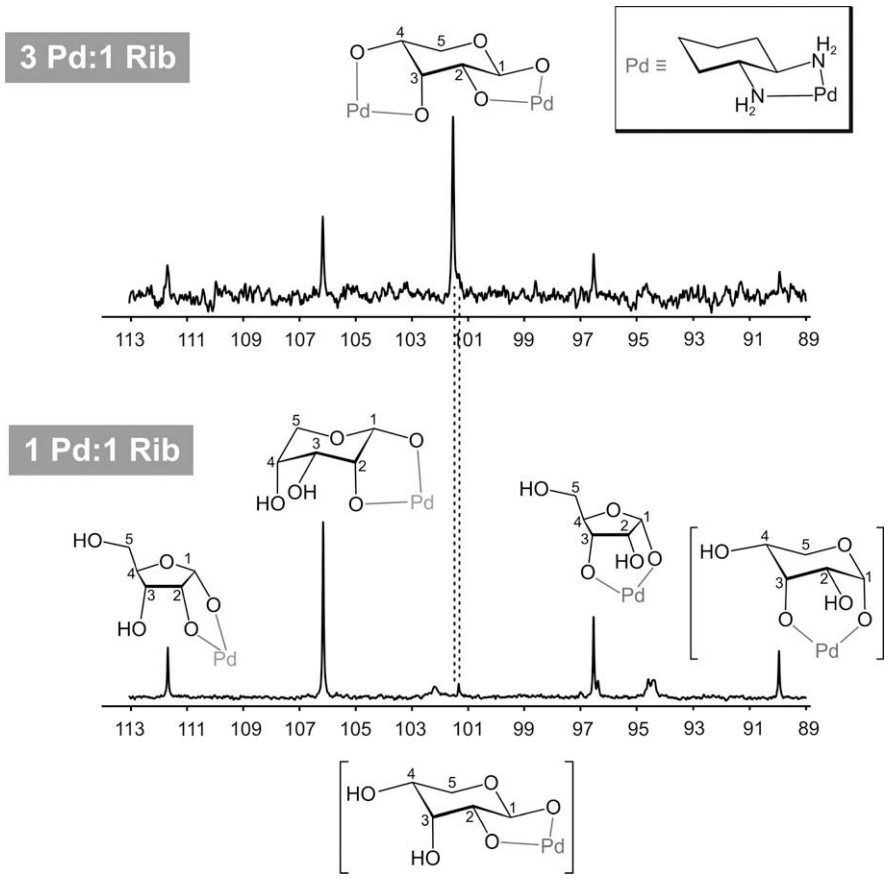

Figure 1. C1 parts of the ^{13}C NMR spectra of D-ribose in Pd-chxn at a molar Pd:Rib ratio of 1:1 (bottom) and 3:1 (top). The formulas given in parentheses are speculative. Dotted lines: see text. The relative amount of the monometallated species in the equimolar solution is, for the four major species, 13%, 52%, 22% and 13% (from left to right).

Table 1
Crystallographic data

	Rib1·2.25H_2O	Xyl1·H_2O	Thr1·2H_2O	Ery1·3H_2O
Empirical formula	$C_{44}H_{106}N_8O_{29}Pd_4$	$C_{11}H_{24}N_2O_6Pd$	$C_{10}H_{24}N_2O_6Pd$	$C_{10}H_{26}N_2O_7Pd$
M_r (g mol^{-1})	1637.03	386.74	374.727	392.743
Crystal size (mm)	0.35 × 0.06 × 0.03	0.35 × 0.06 × 0.04	0.12 × 0.04 × 0.02	0.12 × 0.10 × 0.10
Crystal system	Triclinic	Monoclinic	Monoclinic	Triclinic
Space group	*P*1	$P2_1$	$P2_1$	*P*1
a (Å)	13.2049(5)	8.8523(1)	5.4549(1)	7.4770(2)
b (Å)	13.9351(8)	7.5140(1)	22.9461(6)	10.6050(4)
c (Å)	13.9134(7)	12.0437(2)	11.7928(3)	11.4020(4)
α (°)	64.272(2)	90	90	91.892(2)
β (°)	66.188(2)	97.464(1)	102.5462(8)	109.160(2)
γ (°)	66.188(2)	90	90	110.651(1)
V (Å^3)	2108.3(2)	794.31(2)	1440.84(6)	787.75(5)
Z	1	2	4	2
ρ (g cm^{-3})	1.2894(1)	1.61700(4)	1.7275(1)	1.6558(1)
μ (mm^{-1})	0.906	1.192	1.312	1.208
Absorption correction	Numerical	Numerical	Numerical	None
T_{min}/T_{max}	0.8935/0.9801	0.8698/0.9751	0.8965/0.9722	—
Refls. measured	26347	18827	20269	6581
R_{int}	0.056	0.0461	0.0801	0.0390
Mean $\sigma(I)/I$	0.1157	0.0409	0.1023	0.0513
θ Range	3.1–27.5	3.1–27.5	3.2–27.5	3.8–27.5
Observed refls.	12014	3375	4584	5970
x, *y* (weighting scheme)	0.1740, 11.6777	0.0413, 0.3684	0.0363, 0	0.0355, 0.3528
Flack parameter	0.04(6)	0.00(4)	0.00(3)	−0.04(3)
Refls. in refinement	17010	3641	6207	6581
Parameters	706	191	371	399
Restraints	3	4	13	21
$R(F_{obs})$	0.147	0.034	0.085	0.039
$R_w(F^2)$	0.300	0.075	0.095	0.072
S	1.051	1.071	1.004	1.046
Shift/error$_{max}$	0.001	0.001	0.001	0.001
Max. res. density (e Å^{-3})	2.572	1.343	0.942	0.977
Min. res. density (e Å^{-3})	−0.980	−0.570	−0.726	−0.827

Table 2
^{13}C NMR chemical shifts and CIS values of aldopentose ligands that are verified by a coupling-constant-based analysis

	C1	C2	C3	C4	C5	Glycose isomer	Chelating site(s)
Ara1	105.1	84.6	84.2	78.6	67.1	$^4C_1$-α-L-Ara*p*	κ*O*^{1,2}:κ*O*^{3,4}
	7.7	**12.1**	**11.1**	**11.6**	4.0		
Ara2	103.2	80.6	71.4	68.7	62.4	$^1C_4$-β-L-Ara*p*	κ*O*^{1,2}
	10.0	**11.5**	2.2	−0.6	−0.7		
Ara3	104.0	83.9	82.0	72.9	64.7	$^1C_4$-β-L-Ara*p*	κ*O*^{1,2}:κ*O*^{3,4}
	7.4	**14.8**	**12.8**	**3.6**	1.6		
Ara4	104.4	82.2	77.0	88.9	62.5	α-L-Ara*f*	κ*O*^{1,3}
	2.7	0.1	**0.8**	6.3	0.8		
Ara5	110.4	88.5	78.3	81.9	62.9	β-L-Ara*f*	κ*O*^{1,2}
	14.6	**11.7**	3.5	−0.1	1.2		
Rib1	106.3	83.6	70.2	67.1	66.5	$^1C_4$-α-D-Rib*p*	κ*O*^{1,2}
	12.2	**12.9**	0.4	−0.9	3.0		
Rib2	101.7	82.0	84.0	77.1	66.4	$^4C_1$-β-D-Rib*p*	κ*O*^{1,2}:κ*O*^{3,4}
	7.3	**10.4**	**14.4**	**9.3**	2.8		
Rib3	96.7	73.0	70.6	87.2	62.7	α-D-Rib*f*	κ*O*^{1,3}
	−0.2	1.5	**0.0**	3.6	0.8		
Rib4	111.9	82.8	67.7	80.9	62.1	α-D-Rib*f*	κ*O*^{1,2}
	15.0	**11.3**	−2.9	−2.7	0.2		
Xyl1	102.9	81.3	73.9	69.2	63.1	$^4C_1$-α-D-Xyl*p*	κ*O*^{1,2}
	10.1	**9.2**	0.5	−0.8	1.5		
Xyl2	102.4	83.5	86.5	78.9	63.9	$^4C_1$-α-D-Xyl*p*	κ*O*^{1,2}:κ*O*^{3,4}
	9.6	**11.4**	**13.1**	**8.9**	2.3		
Xyl3	106.0	83.8	77.1	70.2	66.5	$^4C_1$-β-D-Xyl*p*	κ*O*^{1,2}
	8.8	**9.1**	0.7	0.4	0.7		
Xyl4	106.8	85.3	87.2	80.1	65.7	$^4C_1$-β-D-Xyl*p*	κ*O*^{1,2}:κ*O*^{3,4}
	9.6	**10.6**	**10.8**	**10.3**	−0.1		
Xyl5	95.8	68.4, 70.6, 74.7			59.3	$^1C_4$-β-D-Xyl*p*	κ*O*^{1,3}:κ*O*^{2,4}
Xyl6	112.5	89.1	78.3	78.9	61.0	α-D-Xyl*f*	κ*O*^{1,2}
	16.4						
Xyl7	111.7	92.0	79.1	81.8	61.3	α-D-Xyl*f*	κ*O*^{1,2}:κ*O*^{3,5}
	15.6						
Xyl8	104.4	83.5	75.5	82.9	62.8	β-D-Xyl*f*	κ*O*^{1,3}
	2.2						

CIS values at metal-binding positions are typed boldface. The short symbols in column 1 refer to the schemes and the supplementary tables. Note that $^4C_1$ is the conformation of free L-Arap.

Table 3
^{13}C NMR chemical shifts and CIS values of aldohexose ligands that are verified by a coupling-constant-based analysis

Suppl.	C1	C2	C3	C4	C5	C6	Glycose isomer	Chelating site(s)
Gal1	102.6	77.0	73.4	71.0	n.d.	n.d.	α-D-Gal*p*	κ*O*^{1,2}
	9.7	**8.0**	3.6	1.1				
Gal2	102.2	83.4	79.3	81.6	71.3	62.5	α-D-Gal*p*	κ*O*^{1,2}:κ*O*^{3,4}
	9.3	**14.4**	**9.5**	**11.7**	0.2	0.7		
Gal3	105.5	81.1	n.d.	n.d.	n.d.	n.d.	β-D-Gal*p*	κ*O*^{1,2}
	8.4	**8.6**						
Gal4	105.5	85.2	85.1	79.8	76.5	62.5	β-D-Gal*p*	κ*O*^{1,2}:κ*O*^{3,4}
	8.4	**12.7**	**11.6**	**10.4**	0.7	0.7		
Gal5	110.4	88.8	79.0	82.9	n.d.	n.d.	α-D-Gal*f*	κ*O*^{1,2}
	14.8	**11.9**	4.2	1.6				
Gal6	104.9	82.4	78.3	88.7	72.1	63.5	β-D-Gal*f*	κ*O*^{1,3}
	3.3	0.0	**1.5**	5.7	0.4	−0.3		
Gal7	105.5	81.3	79.0	88.1	80.7	73.1	β-D-Gal*f*	κ*O*^{1,3}:κ*O*^{5,6}
	3.5	−0.6	**2.7**	5.6	**8.3**	**9.8**		
Glc1	102.4	80.5	77.0	69.7	72.1	61.4	α-D-Glc*p*	κ*O*^{1,2}
	9.7	**8.4**	3.6	−0.6	0.1	0.2		
Glc2	102.7	83.6	86.5	79.2	74.9	61.3	α-D-Glc*p*	κ*O*^{1,2}:κ*O*^{3,4}
	10.0	**11.5**	**13.1**	**8.9**	2.9	0.1		
Glc3	105.0	83.7	77.0	70.1	77.2	61.4	β-D-Glc*p*	κ*O*^{1,2}
	8.5	**9.0**	0.6	−0.1	0.6	0.0		
Glc4	106.2	85.4	87.2	80.5	76.9	61.7	β-D-Glc*p*	κ*O*^{1,2}:κ*O*^{3,4}
	9.7	**10.7**	**10.8**	**10.3**	0.3	0.3		
Man1	94.5	81.5	80.2	70.7	73.0	61.7	α-D-Man*p*	κ*O*^{2,3}
	−0.2	**10.2**	**9.3**	3.2	0.0	0.1		
Man2	106.5	83.1	73.0	67.8	76.0	61.9	β-D-Man*p*	κ*O*^{1,2}
	12.2	**10.2**	−1.7	−0.5	−1.8	−0.8		
Man3	108.2	86.1	84.3	75.5	77.0	62.1	β-D-Man*p*	κ*O*^{1,2}:κ*O*^{3,4}
	13.9	**14.3**	**10.6**	**8.3**	0.2	0.5		

CIS values at metal-binding positions are typed boldface. The short symbols in column 1 refer to the schemes and the Supplementary tables.

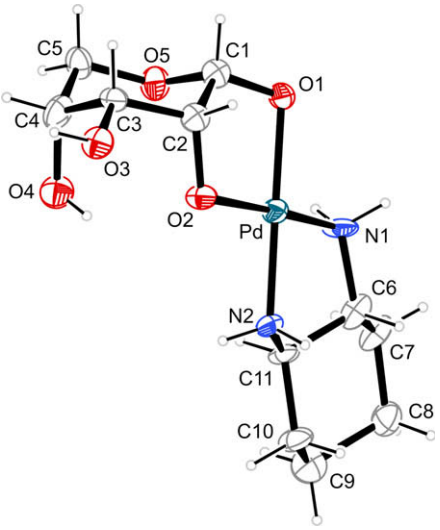

Figure 2. The molecular structure of [Pd{(*R*,*R*)-chxn}($^1C_4$-α-D-Rib*p*1,2H$_{-2}$-κ$O^{1,2}$] in crystals of the 2.25-hydrate. ORTEP plot with 30-% probability ellipsoids. Distances in Å and angles in °: Pd to: O1 2.014(4), O2 2.001(5), N1 2.048(5), N2 2.024(6); O1–Pd–O2 84.4(2), N1–Pd-N2 82.4(2); O1–C1–C2–O2 44.3(5); pyranose puckering (C1–C2–C3–C4–C5–O5): Q = 0.536(5), θ = 10.5(5), φ = 296(2). Intramolecular hydrogen bond O4–H···O2 at a restrained O4–H distance of 0.82: O4···O2 2.65, H···O2 1.93, O4–H···O2 angle 146 (mean of three molecules in the asymmetric unit). Crystallographic data are compiled in Table 1.

($^1C_4$-α-D-Rib*p*1,2H$_{-2}$-κ$O^{1,2}$]·2.25H_2O. The molecular structure is depicted in Figure 2. Agreement with the NMR finding should be noted, including the correctly assigned $^1C_4$ conformation of the ribopyranose ring.

The single-crystal data clarify the reason for the $^1C_4$-α-D-Rib*p*1,2H$_{-2}$-κ$O^{1,2}$ chelation in the major species. A special stabilisation occurs, which, moreover, prevents dimetallation of this particular species. The O4 atom of a *cis*-diol function, the latter usually being prone to being chelated by a second metal atom, establishes an intramolecular O4–H···O2 hydrogen bond. This bond both stabilises the monometallated species and prevents the formation of a dimetallated derivative by impeding further deprotonation and chelation due to decreasing the 4-hydroxyl group's acidity.

To this end, the Pd-chxn solvent, based on a small amount of signal and cross-peak overlap, allows the detection not only of the exhaustively metallated species but also of the more interesting monometallated glycose isomers. Among the monometal derivatives, furanose ligation, which is unusual in a dinuclear complex, is observed. Notably, a furanose is able to form chelates in both the κ$O^{1,2}$ and the κ$O^{1,3}$ modes.

To finish this section, the reader may compare the experimental result and the speculative formulae in Scheme 1. First and most important, all the configurational isomers shown in the scheme were detected experimentally. Hence, a glycose offers a variety of metal-binding sites provided by the members of a dynamic equilibrium. Second, conformational isomerism was determined by intramolecular hydrogen bonding. Third, the single dimetallated species detected under metal-excess conditions is derived from a trace component of the equimolar solution. In particular, the latter point demonstrates that the investigation of a glycose's mono- and dimetallation product represents different aspects of carbohydrate–metal chemistry.

2.2. Aldopentose and aldohexose chelation

2.2.1. Analytic strategy

Prior to extending the ribose results to other aldoses, the general experimental strategy to determine the various metallated species is summarised as follows. (1) The number of metal centres bonded to a glycose was determined by varying the solutions' stoichiometry. (2) An attempt was made to assign the signals in the ^1H and ^{13}C NMR spectra by two-dimensional methods. (3) The H–H coupling constants were used to specify the individual isomers by means of Karplus relationships. (4) The coordination-induced shifts were used to identify the metal-binding sites: a noncritical step for 1,2-diolato bonding, more critical for 1,3-diolato bonding due to small CIS values in the latter case. (5) The last step: cross-checking the consistency of the results among the various aldoses. (6) If possible, X-ray work was used to give additional evidence to the derived results.

As a result of the study on Pd-chxn solutions, Tables 2 and 3 specify the recognised species. It should be noted that whether or not this procedure has an unambiguous result does not depend merely on the abundance of the species in question, but, more importantly, signals and cross-peaks free of overlap appear to be the most significant prerequisite. Thus, in this work, we discuss species of low quantity whose assignment is certain as well as main species whose assignment leaves some ambiguity such as the above-mentioned tentative $^4C_1$-β-D-Rib*p*-derived κ$O^{1,3}$ chelator.

2.2.2. Arabinose and galactose

The L-arabinose/D-galactose couple has been chosen to demonstrate the two main differences mentioned between aldopentose and aldohexose chelation. The configuration of the two aldoses in question is the same: L-arabinose is obtained by removing the terminal hydroxymethylene unit (the one with C6) from D-galactose. The investigation of the two aldoses' reaction with the Pd-chxn reagent proceeded in a similarly promising fashion as with ribose. Again, not only the more distinct full-metallation case could be analysed but also speciation in equimolar solution was unravelled. The result is summarised in Scheme 2.

In equimolar Pd-chxn solutions, arabinose and ribose chelating was closely related. The arabinose's major chelating site had the same environment about the κ$O^{1,2}$-metal-binding site as ribose, but reversed configurations at the distant carbons C3 and C4. Both the κ$O^{1,2}$- and the κ$O^{1,3}$-furanose chelators were present as well. The only difference between the two aldopentoses was the absence of an arabinose analogue of the tentative Rib*p*-κ$O^{1,3}$ species which is impossible with the arabinose configuration (in fact, the assignment for ribose gained evidence by this observation).

The extension of arabinose to galactose does not impose any obvious instabilities on the two furanose chelators. In fact, both species were detected in the respective galactose spectra. Moreover, the 1,3-metallated β-D-galactofuranose was the major species at the equimolar ratio. The significance of steric factors is obvious from a comparison of this species with the analogous [Pd{(*R*,*R*)-chxn}(β-D-Glc*f*1,3H$_{-2}$-κ$O^{1,3}$)] species described in the next chapter. The latter species, which was observed in trace amounts only, showed the terminal dihydroxyethyl substituent with C5 and C6 *endo* to the chelate ring and not *exo* as in the major galactose derivative. A marked instability becomes apparent after extending the major arabinose species [Pd{(*R*,*R*)-chxn}($^1C_4$-β-L-Ara*p*1,2H$_{-2}$-κ$O^{1,2}$)] to its D-Gal homologue. The result, [Pd{(*R*,*R*)-chxn}($^1C_4$-α-D-Gal*p*1,2H$_{-2}$-κ$O^{1,2}$)], resembles a 6-axial conformation. In agreement with the instability of this conformer, its ring-inverted isomer was found in the 1:1 Pd:Gal solutions instead, together with the β-analogue of this species. However, the concentrations of the individual galactopyranose species were lower, since they were derived from an arabinose conformer which was not preferred. (Note again the contrast to the xylose/glucose couple of the next chapter. No instability was introduced there by deriving the major monometallated glucose species from its xylose homologue by the addition of an *equatorial* 6-hydroxymethyl function.)

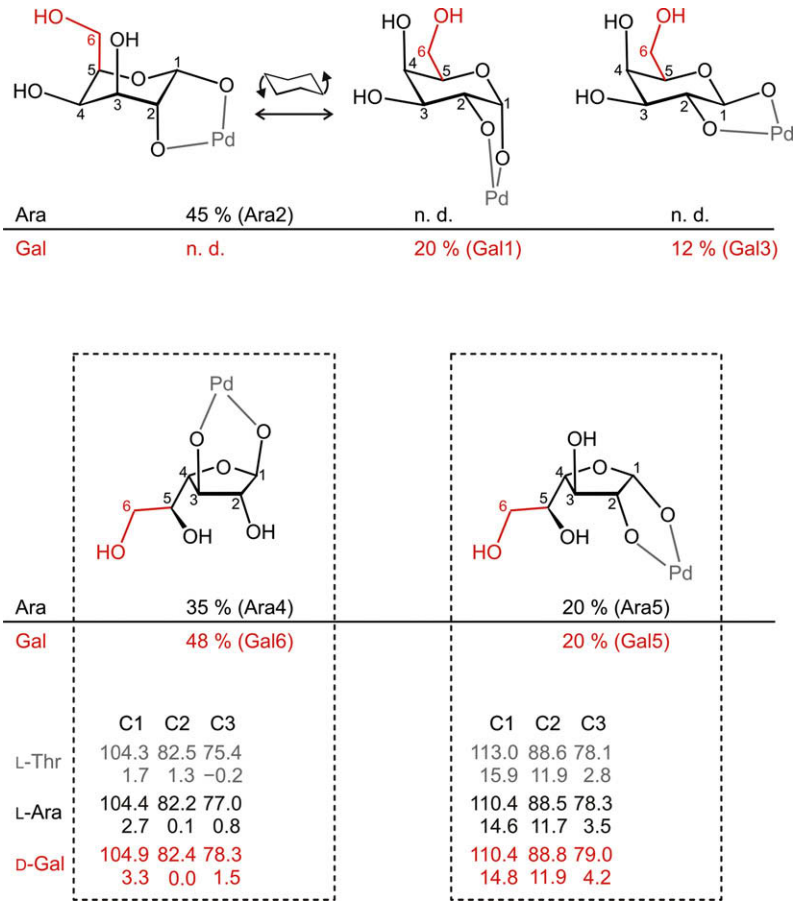

Scheme 2. Monometallated species detected in Pd-chxn solutions of arabinose and D-galactose. The percent values give the relative amount of monometallated species in equimolar solutions. The short symbols for the species refer to the (Supplementary) tables. Formulas and shifts are given for L-arabinose. Coupling constants (Supplementary data) and solution composition refer to D-arabinose. The chemical shifts given for the furanoses are explained in the text. 'Pd' means the {Pd(*R*,*R*)-chxn} fragment (see Fig. 1).

At a 3:1 molar ratio of Pd-chxn and galactose, results were obtained which were similar to those for the Pd-en reagent. Hence, as a rule, a pentofuranose chelator vanishes under full-metallation conditions if it cannot provide a second chelating site—which was the case with arabinose. As another rule, furanose forms vanish from metal-excess aldohexose solutions in favour of $\kappa O^{1,2}$:$\kappa O^{3,4}$-bonded pyranoses. Galactose is the only common aldohexose which is an exception to this rule, forming a dimetallated furanose chelator as a result of an intramolecular O2–H···O5 hydrogen bond. Under such special circumstances only, the additional functional group of a hexose results in an additional metal-binding site.

We were not able to support our species assignment by X-ray work on monometallated arabinose or galactose. Among the dimetallated species, a related species with D-arabinose was crystallised; $[\{Pd(R,R\text{-chxn})\}_2(\beta\text{-D-Ara}pH_{-4}\text{-}\kappa O^{1,2}\text{:}\kappa O^{3,4})]\cdot 10H_2O$, which is completely analogous to the respective complex from Pd-en. It should thus be noted that further evidence on the assigned species was gained from consistency checks. As an example, one of such checks, including data compiled from Tables 2–4, is given in Scheme 2 for the furanose chelators. Resembling well-established experience from NMR work on carbohydrates, the metal complexes also showed similar chemical shifts for isostructural molecular fragments. Accordingly, the same then holds for the respective CIS values. In agreement with this experience, a very close resemblance of the non-terminal carbons' shifts and/or CISs throughout the series L-threose/L-arabinose/D-galactose was observed, and, conversely, confirmed the assigments made (L-threose is 5-deoxymethylene-L-arabinose, see below).

2.2.3. Xylose and glucose

Supplementing the Pd-en solvent by Pd-chxn led to particularly well-resolved spectra in the case of xylose. Among the aldopentoses and hexoses of this work, xylose was the most completely analysed one: even the weak signals of minor species could be included in the analysis.

Due to the prevalence of the two pyranoses as a consequence of the all-equatorial pattern of the non-anomeric hydroxyls, an aque-

Table 4
^{13}C NMR chemical shifts and CIS values of aldotetrose ligands

Suppl.	C1	C2	C3	C4	Glycose isomer	Chelating site(s)
Thr1	104.3	82.5	75.4	76.0	α-L-Thr*f*	$\kappa O^{1,3}$
	1.7	1.3	**−0.2**	2.6		
Thr2	113.0	88.6	78.1	71.4	β-L-Thr*f*	$\kappa O^{1,2}$
	15.9	**11.9**	2.8	0.5		
Ery1	96.1	74.0	69.1	74.5	α-D-Ery*f*	$\kappa O^{1,3}$
	0.0	2.3	**−0.7**	2.6		
Ery2	112.0	82.7	71.0	69.4	α-D-Ery*f*	$\kappa O^{1,2}$
	16.0	**11.0**	1.1	−1.4		
Ery3	98.9	83.3	85.5	72.1	α-D-Ery*f*	$\kappa O^{2,3}$
	2.8	**11.5**	**16.0**	0.1		
Ery4	103.5	89.2	82.9	73.0	β-D-Ery*f*	$\kappa O^{2,3}$
	1.8	**12.3**	**12.0**	1.4		
Ery5	101.7	85.0	83.0	73.8	(1*R*)-D-Ery*h*	$\kappa O^{1,2}$:$\kappa O^{3,4}$
	11.7	**10.9**	**10.8**	**10.7**		
Ery6	100.4	84.6	82.1	74.4	(1*S*)-D-Ery*h*	$\kappa O^{1,2}$:$\kappa O^{3,4}$
	10.3	**10.5**	**9.9**	**11.3**		

CIS values at metal-binding positions are typed boldface. The short symbols in column 1 refer to the schemes and the Supplementary tables.

ous xylose solution showed α- and β-xylopyranose as the only species in a standard ^{13}C NMR experiment. Accordingly, the study of metal-excess Pd-en/xylose solutions had led to the identification of the expected Pd_2 derivatives of the two pyranoses only.[2] Thus, surprisingly, both mono- and dimetallated furanose ligands were detected in addition to the expected species by an analysis of 1:1 and 3:1 Pd-chxn:Xyl solutions. In terms of the degree of metallation, xylose showed the usual 'true-to-stoichiometry' behaviour, to which ribose was an exception. Thus, all the stronger signals of equimolar solutions resembled monometallated species, and all the stronger signals at the 3:1 ratio of Pd-chxn and xylose belonged to dimetallated species.

Four major species were assigned in equimolar solutions (Scheme 3). Two of them were the expected $^4C_1$-α- and -β-D-Xyl*p*1,2H$_{-2}$-κ$O^{1,2}$ chelates which were accompanied by minor amounts of analogous species that, obviously, binded the metal atoms in the κ$O^{2,3}$ and the κ$O^{3,4}$ modes, thus leaving the anomeric hydroxyl unbonded. We will discuss such species in detail after the treatment of the lyxose/mannose couple.

The rule of thumb, that if crystallisation succeeds at all, the major solution species will crystallise, holds for xylose. Figure 3 thus shows the structure of the α-configured chelate in crystals of the monohydrate.

Resembling those of ribose and arabinose, both the Xyl*f*-κ$O^{1,2}$ and the Xyl*f*-κ$O^{1,3}$ furanose ligands were found in the solution state. Due to the stereochemistry of D-xylose, the former is derived from α-Xyl*f* and the latter is derived from β-Xyl*f*. Among the furanose chelators of ribose, arabinose and xylose, the α-D-Xyl*f*-κ$O^{1,2}$ ligand was unique, as it was the only one whose stereochemistry permitted double metallation. In fact, only the monometallated β-Xyl*f*-κ$O^{1,3}$ species vanished on adjusting a 3:1 molar ratio of metal and xylose. The remaining three major species of the equimolar solution, including the unique α-D-Xyl*f* chelator, were transformed to dinuclear species. Two of them are the analogues of the dimetallated pyranoses that had been detected in Pd-en solutions, accompanied by a third signal of the dimetallated α-D-Xyl*f*-κ$O^{1,2}$:κ$O^{3,5}$ ligand.

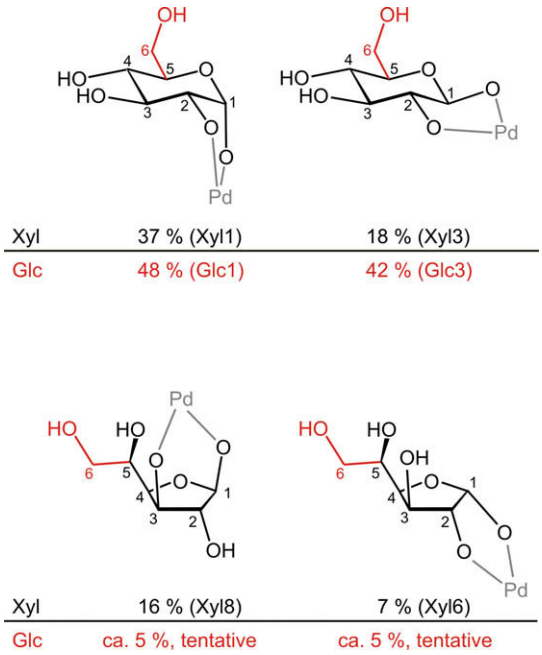

Scheme 3. The major species of equimolar solutions of D-xylose or D-glucose in Pd-chxn. The percent values give the relative amount of monometallated species in equimolar solutions. The short symbols for the species refer to the (Supplementary) tables. Monometallated minor species are the 2,3- and 3,4-monometallated pyranoses (see text). 'Pd' means the {Pd(*R*,*R*)-chxn} fragment (see Fig. 1).

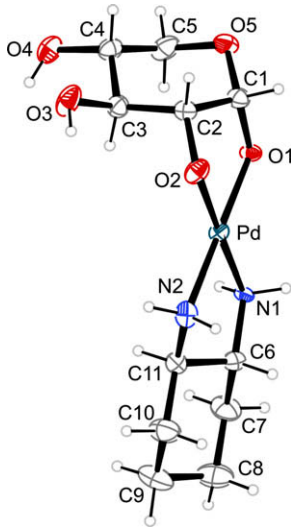

Figure 3. The molecular structure of [Pd{(*R*,*R*)-chxn}(α-D-Xyl*p*1,2H$_{-2}$-κ$O^{1,2}$] in crystals of the monohydrate. ORTEP plot with 50-% probability ellipsoids. Distances [Å] and angles [°]: from Pd to: O1 2.014(4), O2 2.001(5), N1 2.048(5), N2 2.024(6); O1–Pd–O2 84.4(2), N1–Pd–N2 82.4(2); O1–C1–C2–O2 44.3(5); pyranose puckering parameters:[6] Q = 0.536(5) Å, θ = 10.5(5)°, φ = 296(2)°.

Metal-excess xylose solutions showed another remarkable feature: Pd-en and Pd-chxn solutions of aldoses needed a few minutes for equilibration due to some kinetic inertness in ligand substitution. (The benefit of the somewhat slow ligand exchange is that palladium-bonded aldose ligands give rise to sharp NMR signals since there is no ligand exchange on the NMR time scale.) Accordingly, all the signals but one developed completely after about 10 min at the latest. The only exception to this experience was the signals of a fourth species at the 3:1 molar ratio which needed about a day to almost reach their final intensity. Configuration and conformation analysis revealed that an isomer of the dimetallated derivative of the β-D-Xyl*p* ligand had formed. Whereas the more quickly developing isomer was the all-equatorial form $^4C_1$-β-D-Xyl*p*H$_{-4}$-κ$O^{1,2}$:κ$O^{3,4}$, its slowly forming isomer was based on the all-axial ligand in $^1C_4$-β-D-Xyl*p*H$_{-4}$-κ$O^{1,3}$:κ$O^{2,4}$ (Scheme 4). The reason for the lengthened reaction times in the case of the all-axial derivative reflected the energetical situation. Since the metallation patterns of the two isomers were different (bis-1,2-diol vs bis-1,3-diol binding), the all-axial complex could not be formed via the ring inversion of the all-equatorial form, but at least one Pd–O bond per chelate ring needed to be broken prior to ring inversion. If, alternatively, the formation of the all-axial complex was assumed to start from the free ligand, the unfavourably high energy of the $^1C_4$-xylose chair had to be taken into account. In a free-enthalpy relationship, an assumed instability of, say, about

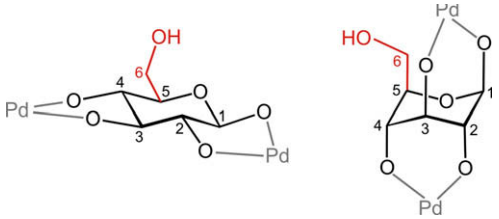

Scheme 4. The two isomeric dimetallated β-D-xylopyranose complexes (C1 to C5 part of the formulae). The 6-hydroxymethyl group extends xylose to glucose; see text for further comments. 'Pd' means the {Pd(*R*,*R*)-chxn} fragment (see Fig. 1).

40 kJ mol^{-1} with respect to the $^4C_1$ chair corresponded to a concentration so low that complex formation was markedly slowed down by this bottleneck.

The extension of xylose to glucose resembled that of the arabinose-galactose couple. No destabilising factors became apparent by the addition of the glucose's terminal hydroxymethylene function to the various monometallated xylose complexes (Scheme 3). Accordingly, all the Pd_1-Xyl species were complemented by a homologous glucose complex. However, the marked prevalence of the pyranoses in a glucose solution governed the species distribution in the metal-containing equilibria as well. Thus, some small signals were attributed to the two types of furanose chelator. Their assignment, however, is speculative.

The same held for metal-excess solutions. The two dimetallated $^4C_1$-pyranose complexes governed the equilibrium.[3] Particularly, the all-axial species was suppressed since it would have given rise to an unfavourable axial hydroxymethyl function (Scheme 4). Attempts to enrich this species by replacing glucose by idose, which provides a stabilising equatorial hydroxymethyl group to the all-axial position of the chelating substituents, are in progress.

2.2.4. Lyxose and mannose

Though the outlined experimental strategy was successfully applied to the above-mentioned systems, the lyxose-mannose couple resisted a coupling-constant-based analysis due to multiple signal and cross-peak overlap in both cases. However, experiments with ^{13}C1-enriched mannose led to a satisfying degree of reliability.

Equimolar solutions of D-mannose in Pd-chxn showed two major signal sets in ^{13}C NMR spectra. As expected from mannose's configuration which made a $\kappa O^{1,2}$-chelating $^4C_1$-α-D-Man*p* ligand sterically impossible, the most abundant solution species was derived from the $^4C_1$-β-D-Man*p*1,2H$_{-2}$-$\kappa O^{1,2}$ ligand. The experience with the glycoses dealt with so far led us to expect that a furanose-derived ligand might have contributed the second major species to the solution equilibrium. All the data collected, however, consistently pointed to the $^4C_1$-α-D-Man*p*2,3H$_{-2}$-$\kappa O^{2,3}$ ligand which binds palladium without the participation of the most acidic O1-hydroxy function (Scheme 5). This result was verified by NMR spectroscopy on ^{13}C1-enriched samples which allowed the detection of $^1J_{C1,H1}$ coupling constants as well as the observation of C1–H5 coupling that unambiguously established the pyranose isomer.

Equimolar solutions of D-lyxose contained the analogous species as well as another species which, tentatively, was assigned to a $^1C_4$-β-D-Man*p*1,3H$_{-2}$-$\kappa O^{1,3}$ ligand. However, lyxose turned out to deserve investigation with other metal probes most especially among the aldopentoses.

Metal-excess solutions of both lyxose and mannose in Pd-chxn led to the dimetallated $^4C_1$-β-D-Man*p*1,2,3,4H$_{-4}$-$\kappa O^{1,2}$:$\kappa O^{3,4}$ ligand, thus completely parallelling Pd-en.

2.2.5. Leaving the anomeric position unmetallated

The α-D-Man*p*2,3H$_{-2}$-$\kappa O^{2,3}$ bonding mode depicted in the right part of Scheme 5 obviously gained significance due to the well-known enhancement of the anomeric effect by a 2-axial substituent. Accordingly, no β isomer of this species was detected. At this point, the more general question might be asked; whether species having the anomeric position unmetallated are common to the glycoses' metallation products or whether they require a special stereoelectronic situation such as a 2-axial substituent. It turns out that such species may be tentatively, but sensibly, assumed as common constituents of the equimolar solutions of other glycoses as well. It should be noted, however, that we were not able to detect such species on the sound basis of coupling-constant analyses. As an example, Figure 4 (top) shows the spectral region close to the C1 signal of free xylose's major isomer, the β-D-pyranose. The signal pattern left of the free xylose's signal is typical and may be regarded as part of a signal series of monometallated β-D-pyranose species with increasing down-field shifts. The series starts close to the free-xylose-C1 signal with the signal of a monometallated $\kappa O^{3,4}$ chelator which bonds the metal most distant from the anomeric centre. Further downfield, the signal of a $\kappa O^{2,3}$-binding species is observed. Finally, as a major and well-characterised species, the signal of a $\kappa O^{1,2}$-binding species is markedly shifted outside the depicted range downfield due to its large CIS value since the palladium atom has reached the anomeric centre in this species.

This pattern is extended by an additional signal in the case of a hexose. Figure 4 (bottom) shows the same part for glucose. In agreement with the existence of another tentative β-D-pyranose-derived metal-binding site, the $\kappa O^{4,6}$ chelator, a fourth signal arises in the depicted range. This signal is still closer to the free glycose's signal since the metal atom is still more distant from C1.

Similar patterns, modified by stability considerations, occur with other glycoses. An example is galactose. Since for palladium(II), the coordination of a pyranoidic *cis*-diol function seems to be somewhat more stable than the coordination of a *trans*-diol moiety, a modified pattern is observed. The tentative $\kappa O^{2,3}$ chelator (*trans*) is thus suppressed, whereas the amount of the $\kappa O^{3,4}$ chelator (*cis*) is increased.

However, though a consistent body of data supports such speculations, the reader should keep in mind that the assignments gi-

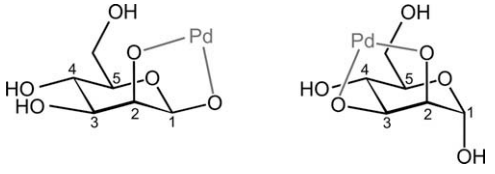

Scheme 5. The two major species of an equimolar solution of D-mannose in Pd-chxn. The relative amounts of the 1,2- and 1,3-chelators are 58% and 42%, respectively. 'Pd' means the {Pd(*R*,*R*)-chxn} fragment (see Fig. 1).

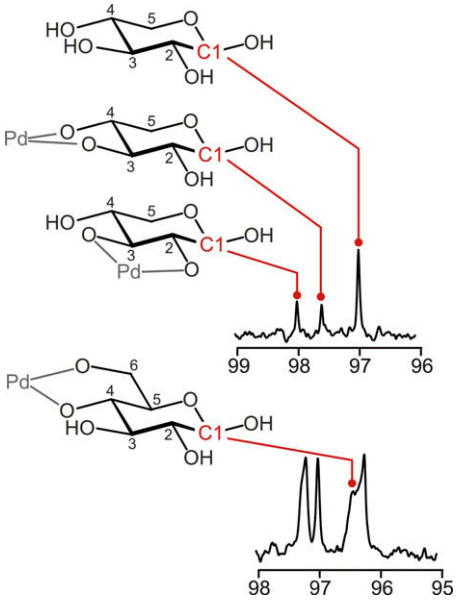

Figure 4. Signals of non-anomerically metallated species in the ^{13}C NMR spectra close to the C1 signal of residual free β-pyranose in equimolar Pd-chxn/glycose solutions of D-xylose (top) and D-glucose (bottom). The common kinds of species are assigned for xylose only. The abundance of these species is 5%, 5%, and 11% of the total glycose content, respectively, for the xylose species from the left to the right signal in the upper spectrum.

ven in this chapter are tentative and are not based on the analysis of correlated spectra.

2.2.6. Aldohexose versus aldopentose binding

In summary, aldohexoses, due to their additional functional group, might have been regarded as ligands with an even more plentiful coordination chemistry than their lighter homologues. However, particularly the common aldohexoses, whose chemistry is dominated by pyranose forms rich in equatorial substituents, were characterised by a restricted molecular flexibility due to the stereoelectronic requirements of a hexose's terminal hydroxymethyl function. The conformational flexibility of a pyranose with respect to ring inversion between $^4C_1$ and $^1C_4$ was thus frozen to the conformer that bears the terminal hydroxymethyl function in the equatorial position.

2.3. Aldotetrose chelation

2.3.1. Threose

The $\kappa O^{1,3}$ bonding mode was the most significant palladium-chelating mode of a furanose. Since CIS values derived from chelates with six-membered rings were less indicative of metal binding than in the case of their five-membered-ring counterparts, additional support of the assignment seems desirable. A straightforward way to shed light on furanose chelation is the investigation of the tetroses, threose (Thr) and erythrose (Ery), which are intrinsically unable to form a pyranose. Choosing either D-xylose or L-arabinose as a starting point, removal of C5 leads to L-threose. Its simple metallation pattern could be predicted by deleting all the pyranoses from the xylose or arabinose chelators lists, thus leaving only the two furanose chelators each. In all cases, the exocyclic 5-hydroxymethyl function was not involved in metal binding. Hence, considering the higher abundance of the $\kappa O^{1,3}$-bonding furanoses, the [Pd{(*R*,*R*)-chxn}(α-L-Thr*f*1,3H$_{-2}$-$\kappa O^{1,3}$)] complex was now expected to develop as the major, and thus, hopefully, crystallisable, solution species. One complication, however, could have been expected: aqueous solutions of L-threose contain 88% furanoses, but also contain 2% open-chain aldehyde and 10% open-chain aldehyde hydrate, the latter two numbers being markedly higher than for the heavier homologues (Scheme 6). It was thus unclear from the beginning whether or not metallation would suppress or enhance threose's open-chain forms.

Equimolar as well as metal-excess solutions of L-threose, in fact, gave rise to two signal sets of the expected furanose chelators with the attempted $\kappa O^{1,3}$-chelate as the major species (56% $\kappa O^{1,3}$ and 44% $\kappa O^{1,2}$ chelate). Open-chain isomers were suppressed in terms of NMR spectroscopy. Attempts to crystallise the major species resulted in the isolation of its dihydrate, [Pd{(*R*,*R*)-chxn}(α-L-Thr*f*1,3H$_{-2}$-$\kappa O^{1,3}$)]·2H$_2$O. The structure verified the NMR result including the prediction from the $^3J_{H,H}$ coupling constants that the conformation should be close to $^3T_2$ or E_2 (Fig. 5 shows one of two symmetrically independent molecules).

It should be noted that the successful structure determination clearly illustrated a general problem of carbohydrate chemistry and, in particular, of the chemistry of the carbohydrates' metal derivatives, namely the tendency to form syrups instead of crystals. Hence, the palladium–threose complex was the first-ever crystal structure of a tetrose, either metallated or non-metallated. In terms of the Cambridge data base, only few tetroside structures are known.

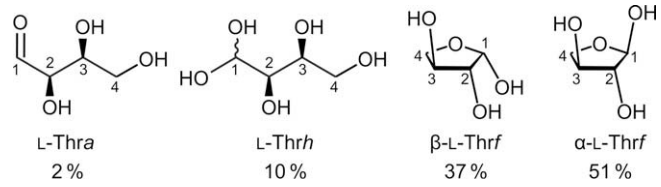

Scheme 6. Solution species and percent distribution of L-threose in an aqueous equilibrium. Percent amounts are taken from Refs. 7 and 8.

2.3.2. Erythrose

Unexpectedly, in terms of the closely related species distributions in the tetroses' aqueous equilibria, the same experiments ended up with a different outcome for erythrose, the epimeric tetrose, which was investigated in its D form (2% aldehyde, 10% aldehyde hydrate, 25% α-, 63% β-furanose). Equimolar and metal-excess conditions now led to different spectra. At the 1:1 molar ratio of metal probe and glycose, NMR analysis showed the expected result, namely three mononuclear species derived from the three possible chelators (given in the order of species abundance): the α-D-Ery*f*1,3H$_{-2}$-$\kappa O^{1,3}$ and the α-D-Ery*f*1,2H$_{-2}$-$\kappa O^{1,2}$ form, and, in addition to the threose-derived chelators, the D-Ery*f*2,3H$_{-2}$-$\kappa O^{2,3}$ anomers. (A threose analogue of the latter was not expected due to the unfavourable chelating properties of a *trans*-furanose.)

At a 3:1 molar ratio of Pd:Ery, the difference between threose and erythrose spectra became pronounced. Figure 6 shows the assigned ^{13}C NMR spectrum at a 3:1 Pd:D-Ery molar ratio. Two new features are notable: first, the anomeric pair of the D-Ery*f*2,3H$_{-2}$-$\kappa O^{2,3}$-derived species showed broadened C1 and C2 signals due to accelerated mutarotation at the higher pH value (note that 3 mol of the metal reagent carries 6 mol of hydroxide). The second feature was more interesting. Though the open-chain hydrate had disappeared on metal addition in the case of threose, it was enriched to about twice the content of a metal-free solution in the case of erythrose. In terms of CIS values, the open-chain hydrate acted as a bis(diolato) ligand. The exchange of the two geminal hydroxy groups at the C1 atom was slow on the NMR time scale so that two separate sets of four signals were observed for the dimetallated, tetra-anionic, open-chain glycose hydrate.

The reason for the suppression of the open-chain threose, but the enrichment of the erythrose's aldehyde hydrate, is explained by scrutinising the chemistry of the actual metal-binding part of the open-chain erythrose hydrate. Replacing the non-Pd-bonding

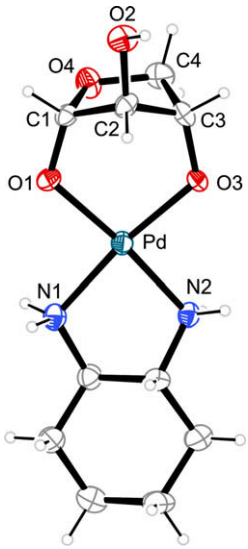

Figure 5. The molecular structure of one of two symmetrically independent molecules of [Pd{(*R*,*R*)-chxn}(α-L-Thr*f*1,3H$_{-2}$-$\kappa O^{1,3}$)] in crystals of the dihydrate (50% ellipsoid probability). Distances [Å] and angles [°]: molecule 1: from Pd to: O1 2.013(4), O3 2.009(4), N1 2.050(5), N2 2.019(5); O1–Pd–O3 96.2(2); molecule 2: from Pd to: O1 2.002(4), O3 2.010(4), N1 2.043(5), N2 2.027(5); O1–Pd–O3 95.8(2).

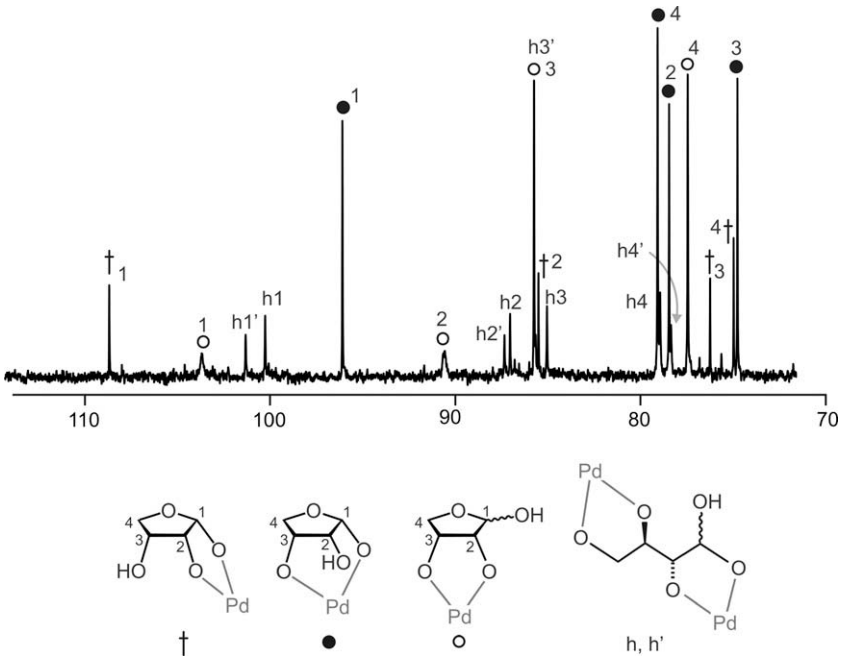

Figure 6. The ^{13}C NMR spectrum of D-erythrose in [Pd^{II}{(*R*,*R*)-chxn}$(OD)_2$]/D_2O at a 3:1 molar ratio of Pd:D-Ery. Note coalescence of the α- and β-signals of the C1 and C2 atoms of the mutarotating D-Ery*f*2,3H$_{-2}$-κ$O^{2,3}$ ligand (open circles). 'Pd' means the {Pd(*R*,*R*)-chxn} fragment (see Fig. 1).

hydroxy group by a hydrogen atom, the sugar alcohol erythritol is obtained. Accordingly, the Pd-bonding capabilities of the isomeric tetraols erythritol and threitol were distinct and matched the finding in this work. While threitol formed a stable monometallated 2,3-bonded complex both in Pd-en and in Pd-chxn, but showed only a limited tendency towards dimetallation, the coordination chemistry of the *meso* compound erythritol was determined by the high formation tendency of the centrosymmetric dimetallated bonding pattern. Obviously, the coordination chemistry of an open-chain hydrate follows the rules derived for the actually metal-binding part of the molecule, the open-chain sugar alcohols.[9]

The crystallisation of erythrose-containing species was successful for the equimolar solutions and resulted in the isolation of the major species's trihydrate [Pd(*R*,*R*-chxn)(α-D-Ery*f*1,3H$_{-2}$-κ$O^{1,3}$)]·3H_2O. Again, the spectroscopic assignment of a furanose's κ$O^{1,3}$ bonding mode was confirmed by structural work (Fig. 7).

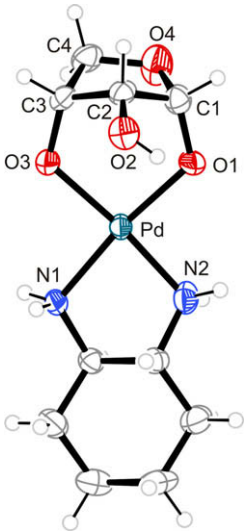

Figure 7. The molecular structure of one of two symmetrically independent molecules of [Pd(*R*,*R*-chxn)(α-D-Ery*f*1,3H$_{-2}$-κ$O^{1,3}$)] in crystals of trihydrate (50% ellipsoid probability). Distances [Å] and angles [°]: molecule 1: from Pd to: O1 1.991(5), O3 2.012(5), N1 2.056(6), N2 2.014(7); O1–Pd–O3 95.9(2); molecule 2: from Pd to: O1 1.996(5), O3 2.019(5), N1 2.011(6), N2 2.053(6); O1–Pd–O3 95.7(2).

3. Conclusions

The cellulose solvent Pd-en, an aqueous solution of [Pd(en)$(OH)_2$], provided a first insight into the coordination chemistry of the aldoses. Due to the experimental conditions such as the thermal instability of the glycose solutions or signal and cross-peak overlap, the use of Pd-en was limited to metal-excess solutions which, as a rule, contain fewer species compared to equimolar solutions. Under metal-excess conditions, dimetallated κ$O^{1,2}$:κ$O^{3,4}$-binding pyranoses were observed with the exception of galactose only, which showed a furanose-derived binuclear furanose species stabilised by intramolecular hydrogen bonding.

Pd-chxn, an aqueous solution of [Pd{(*R*,*R*)-chxn}$(OH)_2$], allowed the investigation of solutions equimolar with respect to palladium and aldose. The experimental background of this progress was the slightly enhanced thermal stability of the solutions and less signal and cross-peak overlap for the aldoses presented in this work except for lyxose and mannose.

As a result, the use of the new palladium probe revealed rules regarding the particularly fundamental bonding mode of a ligand, namely bidentate chelation. These general rules include (1) a preference for the participation of the most acidic, anomeric hydroxyl group to the chelate rings. With the exception of lyxose and mannose, chelates that leave O1 unbonded, are minor species. (2) No serious limitations are apparent with respect to the stereochemistry of the chelate-providing backbone. Thus not only the pyranoses contribute to the chelator set but also both *cis*-1,2-furanose and *cis*-1,3-furanose chelation are observed. (3) The *cis*-1,3-bonding mode is the most significant mode for a furanose, whereas 1,3-chelation is restricted to special cases for a pyranose since the often unstable 1,3-diaxial pattern is a prerequisite.

Keeping in mind the dynamic nature of an aldose's equilibrium mixture, an individual aldose thus provides numerous ligand isomers in the sense of a dynamic ligand library. The well-resolved

cases of this work clearly demonstrate that the often limited species diversity in an aldose's aqueous solution markedly increases and provides various ligand types to a metal, including such unexpected isomers as an all-axial-pyranose and open-chain forms.

The ligand libraries of an aldopentose and an aldohexose are of about the same complexity. Though an aldohexose provides an additional potentially metal-binding hydroxy function, library members appear to be excluded if a pyranose conformation with an axial 6-hydroxymethyl substituent is adopted.

This study underlines that palladium(II) appears to be a 'non-compelling' centre in the sense that the glycose molecule was not forced into an unusual conformation by the action of a single metal atom. Thus, for the moment, there is no hint of pyranose boats on palladium. It should be noted that the unfavourable all-axial conformation of the xylopyranose ligand was stabilised by the cooperation of two metal atoms. For a more demanding metal centre, the addition of further conformers of a glycose to its increasing ligand library may be expected.

4. Experimental

4.1. Methods and materials

Reagent grade chemicals were purchased from Aldrich, Merck, Fluka or Omicron and were used as supplied. The synthesis of [Pd(*R*,*R*-chxn)Cl_2] relies on the procedure given in Ref. 10 The synthesis of [Pd(*R*,*R*-chxn)$(OH)_2$] was carried out under an atmosphere of nitrogen using standard Schlenk techniques. All Pd(*R*,*R*-chxn)/carbohydrate complexes were prepared under air atmosphere and ice-bath cooling. To obtain the yellow crystals in a good quality, crystallisation was interrupted typically at a yield of 10%.

The elemental analyses were collected on a Elementar Vario EL Apparatur.

4.2. Spectroscopy

NMR spectra were recorded at room temperature (4 °C for erythrose samples) on a Jeol Eclipse 270 (^{1}H: 270 MHz, ^{13}C{^{1}H}: 67.9 MHz), a Jeol Eclipse 400 (^{1}H: 400 MHz, ^{13}C{^{1}H}: 101 MHz) NMR or a Jeol 500 Eclipse spectrometer (500.16 MHz for ^{1}H; 125.77 MHz for ^{13}C) spectrometers. The signals of the deuterated solvent (^{13}C{^{1}H}) and the residual protons therein (^{1}H) were used as an internal secondary reference for the chemical shift. When D_2O was used as a solvent, either one drop of acetone or a small capillary tube containing DMSO-d_6 was added to the sample tube (5 mm) in order to obtain a reference signal in the ^{13}C{^{1}H} NMR spectra. When necessary, the ^{1}H and ^{13}C{^{1}H} NMR signals were assigned by means of ^{1}H–^{1}H-COSY45, DEPT135, TOCSY, ^{1}H–^{13}C-HMQC and ^{1}H–^{13}C-HMBC experiments in solutions of [Pd(*R*,*R*-chxn)$(OD)_2$] (0.5 M) in D_2O. Shift differences are given as $\delta(C_{complex}) - \delta(C_{free\ sugar})$. The values for the free sugars are determined for the respective sugar in its neutral aqueous solution, and were referenced to 49.5 ppm for the ^{13}C NMR signal of methanol.

Mass spectra were measured on a Thermo Finnigan LTQ FT with IonMax (ion source with ESI head).

4.3. [Pd(*R*,*R*-chxn)Cl_2]

To a suspension of $PdCl_2$ (5.00 g, 28.2 mmol) in water (50 mL) at 45 °C was added KCl (4.20 g, 56.3 mmol) , and the mixture was stirred for 10 min until a brown solution of $K_2[PdCl_4]$ was formed. (1*R*,2*R*)-Diaminocyclohexane (3.22 g, 28.2 mmol) dissolved in HCl (100 mL, 0.5 M) was slowly added. After the reaction mixture was stirred for 1 h at 45 °C, the pH was raised with a solution of NaOH (1 M) to 7.0, and the yellow complex precipitated from the solution. The reaction mixture was stirred for other 3 h at 45 °C, (during the first hour, the pH value was repeatedly adjusted). After the suspension was cooled to room temperature the yellow complex was filtered through a G4 filter, washed with cold water (5×30 mL) and dried in vacuo over $CaCl_2$. The yield was 7.81 mg (95%). Anal. Calcd for $C_6H_{14}Cl_2N_2Pd$: C, 24.72; H, 4.84; N, 9.61; Cl, 24.32. Found: C, 24.64; H, 4.78; N, 9.57; Cl, 24.20. ^{13}C{^{1}H} NMR (100.63 MHz, DMSO-d_6): δ 23.7 (2C, γ-CH_2), 32.2 (2C, β-CH_2), 61.0 (2C, α-CH_2).

4.4. [Pd(*R*,*R*-chxn)$(OH)_2$] (0.3 M)

[Pd(*R*,*R*-chxn)Cl_2] (1.75 g, 6.00 mmol), Ag_2O (1.45 g, 6.26 mmol) and water (20 mL) were stirred under nitrogen with exclusion of light at 40 °C. After 2 h AgCl was removed by filtration through a G4 filter under nitrogen atmosphere, leaving a yellow solution. Solutions of higher or lower concentration were prepared by varying the amount of water. For the preparation of [Pd(*R*,*R*-chxn)$(OD)_2$] D_2O was used. The alkaline [Pd(*R*,*R*-chxn)$(OH)_2$] solution (pH 12 for 0.3 M) was kept under a nitrogen atmosphere at 4 °C to prevent absorption of carbon dioxide. ^{1}H NMR (400.18 MHz, D_2O): δ 1.02–1.21 (m, 4H, β-CH_2, γ-CH_2), 1.56–1.59 (m, 2H, γ-CH_2), 1.90–1.93 (m, 2H, β-CH_2), 2.32–2.35 (m, 2H, α-CH_2). ^{13}C{^{1}H} NMR (100.63 MHz, D_2O): δ 23.6 (2C, γ-CH_2), 33.0 (2C, β-CH_2), 60.2 (2C, α-CH_2). ^{13}C{^{1}H} NMR (100.63 MHz, H_2O): δ 24.0 (2C, γ-CH_2), 33.5 (2C, β-CH_2), 60.9 (2C, α-CH_2).

4.5. (1*R*,2*R*)-1,2-Diaminocyclohexane(α-D-xylopyranos-1,2-*O*-diato)palladium(II) monohydrate

D-Xylose (76.1 mg, 0.51 mmol) was dissolved in [Pd(*R*,*R*-chxn)$(OH)_2$] (4 mL, 0.28 M, 1.12 mmol), and stirred for 24 h at 4 °C. The solution was saturated with acetone; subsequently, acetone vapours were allowed to diffuse into the solution. Yellow crystals (Xyl1·H_2O) were formed within 5 d at 4 °C.

4.6. (1*R*,2*R*)-1,2-Diaminocyclohexane(α-D-ribopyranos-1,2-*O*-diato)palladium(II) 2.5-hydrate

D-Ribose (0.15 g, 1.00 mmol) was dissolved in [Pd(*R*,*R*-chxn)$(OH)_2$] (2.0 mL, 0.5 M, 1.00 mmol), and stirred for 1 h at 4 °C. 0.4 mL of this solution was saturated with acetone, and covered with a layer of 2 mL ethanol. After 2 days the solution was covered again with 2 mL of ethanol. Yellow crystals were formed within few days at 0 °C. The crystals were very unstable and started to decompose outside the mother liquor in a few seconds.

4.7. (1*R*,2*R*)-1,2-Diaminocyclohexane(α-L-threofuranos-1,3-*O*-diato)palladium(II) dihydrate

L-Threose (48 mg, 0.40 mmol) was dissolved in [Pd{(*R*,*R*)-chxn}$(OH)_2$] (2.4 mL, 0.17 M, 0.41 mmol). The mixture was stirred for 2 h at 0 °C; 0.4 mL of the solution was saturated with acetone and covered with a layer of 2 mL ethanol. Yellow crystals (Thr1·$2H_2O$) were formed within three days.

4.8. (1*R*,2*R*)-1,2-Diaminocyclohexane(α-D-erythrofuranos-1,3-*O*-diato)palladium(II) trihydrate

An aqueous solution of D-erythrose (1 mL, 0.46 M, 0.46 mmol) was added to [Pd{(*R*,*R*)-chxn}$(OH)_2$] (1 mL, 0.5 M, 0.5 mmol). The mixture was stirred for 2 h at 0 °C. The solution was saturated with acetone and covered with a layer of acetone. Yellow crystals (Ery1·$3H_2O$) were formed within four days.

4.9. Crystal-structure determination and refinement

Crystals suitable for X-ray crystallography were selected with the aid of a polarisation microscope, mounted on the tip of a glass fibre and investigated at 200 K on a Nonius KappaCCD diffractometer with graphite-monochromated Mo Kα radiation (λ = 0.71073 Å). Numerical absorption correction (SCALEPACK) was applied.[11] The structures were solved by direct methods (SIR 97) and refined by full-matrix least-squares calculations on F^2 (SHELXL-97). Anisotropic displacement parameters were refined for all non-hydrogen atoms. Crystallographic data are listed in Table 2. The structure determination on Rib1·2.25H_2O is affected by C_2 pseudosymmetry and is preliminary.

CCDC 717729 (ribose), 717730 (xylose), 644336 (threose) and 644337 (erythrose) contain the supplementary crystallographic data for this paper. These data can be obtained free of charge from the Cambridge Crystallographic Data Centre via www.ccdc.cam.ac.uk/data_request/cif.

Acknowledgements

This work was supported by the Deutsche Forschungsgemeinschaft (Grant Kl624/12-1). We are indebted to D. Heß for experimental assistance.

Appendix: Corrected assignments to Pd-en-based species

Some corrections must be made to the assignments given in Ref. 2 in view of the body of data now available. Thus, the tentative assignment of a dimetallated α-Rib*p* species was wrong and must be replaced by its monometallated analogue, the $^1C_4$-α-D-Rib*p*1,2H$_{-2}$-κ$O^{1,2}$ species. Secondly, two signal pairs of two dimetallated galactose species must be adjusted in the former work. Thus, Table 3 shows Gal4-C4 and Gal7-C5 switched with respect to the Pd-en-related work; the same holds for the Gal7-C3 and C4 couple of signals.

Supplementary data

Supplementary data associated with this article can be found, in the online version, at doi:10.1016/j.carres.2009.04.008.

References

1. Allsche, T.; Klüfers, P.; Mayer, P. In *Glycoscience*; Fraser-Reid, B., Tatsuta, K., Thiem, J., Eds.; Springer: Berlin, Heidelberg, 2008; pp 1079–1139. and literature cited therein.
2. Klüfers, P.; Kunte, T. *Chem. Eur. J.* **2003**, *9*, 2013–2018.
3. Klüfers, P.; Kunte, T. *Angew. Chem.* **2001**, *113*, 4356–4358. *Angew. Chem. Int. Ed.* **2001**, *40*, 4210–4212.
4. Klüfers, P.; Mayer, P. *Acta Crystallogr., Sect. C* **1998**, *54*, 583–586.
5. Ahlrichs, R.; Ballauff, M.; Eichkorn, K.; Hanemann, O.; Kettenbach, G.; Klüfers, P. *Chem. Eur. J.* **1998**, *4*, 835–844.
6. Cremer, D.; Pople, J. A. *J. Am. Chem. Soc.* **1975**, *97*, 1354–1358.
7. Serianni, A. S.; Pierce, J.; Huang, S.-G.; Barker, R. *J. Am. Chem. Soc.* **1982**, *104*, 4037–4044.
8. Serianni, A. S.; Barker, R. *J. Org. Chem.* **1984**, *49*, 3292–3300.
9. Allscher, T.; Kästele, X.; Kettenbach, G.; Klüfers, P.; Kunte, K. *Chem. Asian J.* **2007**, *2*, 1037–1045.
10. Kim, J.-Y. *Arch. Pharm. Res.* **1992**, *15*, 336–342.
11. Otwinowski, Z.; Minor, W. In *Macromolecular Crystallography A*; Carter, C. W., Jr., Sweet, R. M., Eds.; Methods in Enzymology; Academic Press: New York, 1997; Vol. 276, pp 307–326.